ORIGINAL ARTICLE

New index to assess the extent of bone disease in patients with prostate cancer using SPECT/CT

Hajime Ichikawa[1] · Takayuki Shibutani[2] · Masahisa Onoguchi[2] · Yuki Taniguchi[1]

Abstract

Objective Assessing the extent of bone metastases in patients with prostate cancer is very important to predict patient prognosis. Therefore, the bone scan index (BSI), which is easy to use, has been used; however, the accuracy is not that high. In this study, we proposed a new index for the extent of bone disease using single-photon emission computed tomography with computed tomography (SPECT/CT) images and assessed the accuracy of calculation.

Methods In this study, a total of 46 bone scans from 12 patients with prostate cancer treated for bone metastases with Radium-223 were included. Whole-body planar images were obtained 150–180 min after an intravenous injection of ^{99m}Tc-methylene diphosphonate, and cervical-to-pelvic SPECT/CT was immediately obtained. The total bone volume (TBV) and regional metabolic bone volume (MBV) were defined as Hounsfield unit of > 120, standardized uptake value (SUV) of > 0.5, and SUV of > 5–8 in four levels, respectively. Bone metabolism volumetric index (BMVI) was calculated as the percentage of the total MBV divided by TBV. The variability of the TBV measurement was evaluated by the percentage coefficient of variance (%CV) of TBV within individual patients. We evaluated the correlation of TBV with age, height, weight, and body mass index and the correlation and agreement between BSI and BMVI.

Results The mean and %CV of TBV were 4661.7 cm^3 and 2.8%, respectively, and TBV was strongly correlated with body weight. BMVI was significantly higher than BSI and correlated with alkaline phosphatase. For patients with progressive bone metastases, BSI was clearly underestimated, whereas BMVI was elevated.

Conclusions Although assessed in a small number of cases, the new index for assessing the extent of bone disease using SPECT/CT imaging was highly value than BSI and was significantly correlated with alkaline phosphatase. Therefore, this study suggests that BMVI could improve the low sensitivity of BSI in patients with low extent of disease grade.

Keywords Bone scintigraphy · Quantitative single-photon emission computed tomography (SPECT) · Extent of disease (EOD) · Bone scan index (BSI) · Prostate cancer

Introduction

Patients with prostate cancer have an extremely high risk of bone metastasis, and thus, to improve their quality of life, appropriate management of bone metastasis is important. Serum tartrate-resistant acid phosphatase, alkaline phosphatase (ALP), and prostate-specific antigen (PSA) have been known as biochemical markers to predict bone metastasis [1]. As an imaging biomarker, bone scan index (BSI) is calculated as a percentage weight of the total abnormal bone uptake in the entire skeleton using whole-body bone scintigraphy [2–8]. Accurate BSI measurement of the extent of disease (EOD) is more important than accurate counting of the number of bone metastases to determine a patient's prognosis [9]. It can also be used to complement PSA in stratifying the risk in patients with prostate cancer [10]. However, automatic BSI calculation has been underestimated unless corrected by a physician [5], whereas the agreement of diagnosis by physicians using computer-assisted diagnosis is 68 (inexperienced readers) to 75% (experienced readers) [11]. When BSI is $> 1\%$, the incidence

✉ Masahisa Onoguchi
onoguchi@staff.kanazawa-u.ac.jp

1 Department of Radiology, Toyohashi Municipal Hospital, 50 Aza Hachiken Nishi, Aotake-Cho, Toyohashi, Aichi 4418570, Japan

2 Department of Quantum Medical Technology, Graduate School of Medical Sciences, Kanazawa University, 5-11-80 Kodatsuno, Kanazawa, Ishikawa 9200942, Japan

of progression, shortened overall survival, and cancer death increases, then BSI changes are associated with prognosis [10, 12, 13]. Regardless, patients with lower EOD grades have lower sensitivity and specificity of bone metastases and higher variations among observers in visual assessment [14]. These problems should be improved in clinically using EOD.

Although the added interpretation value in computed tomography (CT) images may be considerable, single-photon emission computed tomography with computed tomography (SPECT/CT) has a higher sensitivity for detecting lesions compared with whole-body planar images [15–19]. It is well known that SPECT is superior to planar images for lesion detection and volume assessment [10]. In this regard, an in-house program for automatic lesion detection using SPECT/CT images has been developed but has not been commonly used [20]. This program automatically detects lesions by determining the threshold value of SPECT counts and by performing multiple regressions for each patient based on the standard deviation of SPECT counts. With the recent availability of SPECT/CT, the classification of benign and malignant lesions using the standardized uptake value (SUV) rather than SPECT counts has been investigated. Kuji et al. have demonstrated that the area under the receiver operating characteristic curve of the mean SUV was significantly higher than that of ALP in discriminating between bone metastases and degenerative changes [21]. Changes in the sum of the product of mean SUV and volume of extracted regions with SUV of ≥ 7 (total bone uptake [TBU]) using a freeware were found to be more accurate and sensitive than BSI [22]. This software-based method is advantageous, because regions can be extracted by setting threshold values for the Hounsfield unit and SUV, respectively. Although much evidence has been established on the validity of assessing the EOD, mainly BSI, very little evidence has been established on TBU.

Therefore, we investigated a new index for assessing the volumetric extent of bone disease to accurately determine the volume of bone disease by measuring the volume of entire the skeleton and bone lesions using SPECT/CT images. In the present study, the variability of measuring the entire skeletal volume and the relationship between the new index and BSI and ALP were assessed.

Materials and methods

Patients

A total of 46 bone scans obtained from 12 patients with prostate cancer (median age, 74 [range, 64–85] years; height, 167 [range, 155–171] cm; weight, 72.4 [range, 45.1–81.0] kg; and body mass index [BMI], 25.7 [range, 18.8–29.4] kg/m^2) who had bone metastases and who were treated with Radium-223 from January 2017 to 2022 were included. The interval between bone scintigraphy and blood tests ranged from 0 to 35 (median 4.5) days, and ALP (normal range, 38–113 U/L) and PSA (normal range, < 4.0 ng/mL) levels were examined. The median number of bone scintigraphy per patient was 3 (range, 2–9). The ethics committee of our hospital approved the study protocol, and our proposed method was not used in practice because of a retrospective study.

Bone scintigraphy

Bone scintigraphy was performed using a Symbia intevo SPECT/CT system equipped with a low-energy high-resolution collimator (Siemens Healthcare, Erlangen, Germany). The whole-body planar images were obtained 150–180 min after intravenously injecting 555–740 MBq ^{99m}Tc-methylene diphosphonate (PDRadiopharma Inc., Tokyo, Japan), and SPECT/CT of the cervical spine to the pelvis was immediately performed. The whole-body planar images were obtained at a scan speed of 15–17 cm/min. SPECT was performed using the following parameters: energy window, 15% at 140 keV; lower subwindow, 15% for scatter correction; 256×256 matrix and 1.0 zoom (with a 2.4×2.4 mm^2 pixel); 90 views over 360°; 12 s per view; and continuous mode through the noncircular orbit. CT scanning at 130 kVp was performed on a 2.0 mm-thick slice, with dose modulation and quality reference of 40 mAs, pitch 2. CT data were reconstructed using B70 kernels for localization and H08 SPECT AC for CT-based attenuation correction. Quantitative SPECT images were reconstructed using the xSPECT Quant algorithm with manufacturer-specific parameters (1 subset, 48 iterations, and a 10 mm Gaussian smoothing filter at full width at half maximum).

Data analysis

BSI

BSI was calculated using BONENAVI software ver. 2 (EXINI Diagnostics AB, Lund, Sweden and PDRadiopharma Inc., Tokyo, Japan) [7]. A parameter associated with sensitivity, CADx, was set to balance. No operator-assisted manual correction for benign or malignant hot spots was performed.

BMVI

The total bone volume (TBV) and regional metabolic bone volume (MBV) were calculated for cervical spine to pelvis SPECT/CT images using the GI-BONE software (Nihon Medi-Physics Co. Ltd., Tokyo, Japan). Figure 1 shows the extracted TBV and total MBV and the bone metabolism
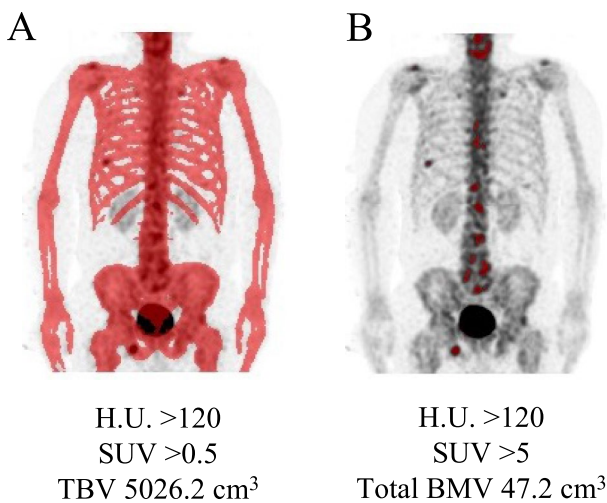
A

B

H.U. >120
SUV >0.5
TBV 5026.2 cm^3

H.U. >120
SUV >5
Total BMV 47.2 cm^3

Fig. 1 Measurement process of TBV and total MBV. Red areas in each image are the extracted regions for respective parameters. The total MBV was calculated from the total volumes of all hot lesions. BMVI was defined as the percentage of the total MBV divided by TBV. The BMVI$_{SUV5}$ in this case was 0.94

volumetric index (BMVI) calculation process. TBV was defined as a region with a Hounsfield unit of > 120 and SUV of > 0.5, thereby eliminating radioactive urine and microcalcifications to improve the accuracy of TBV measurement. The mean SUV of the normal thoracic and lumbar spine in Japanese patients has been reported to be 4.4–4.6, and the SUV threshold value to detect abnormal uptake should be higher than 5 [19, 21]. Regional MBV was also similarly measured in four SUV levels, i.e., > 5, > 6, > 7, and > 8, with a Hounsfield unit of > 120, and the sum of each level was used as the total MBV. The BMVI was calculated as the percentage of the total MBV divided by TBV, that is, the volumetric index for the extent of bone disease. The variability of TBV measurement was evaluated using the percentage coefficient of variance (%CV) of TBV of each patient.

Statistical analysis

Correlations between TBV and age, height, weight, and BMI were evaluated using scatter plots and linear regression models, which were also used to evaluate the correlation between BSI and BMVIs that were calculated with each threshold value, and Bland–Altman plots were created to evaluate the agreement between BSI and BMVIs. Correlations were tested using two-sided Spearman's rank correlation coefficients. After evaluating the nonnormal distribution using the Shapiro–Wilk test, paired values were analyzed using the Wilcoxon signed-rank test. Then, patients were classified into four groups based on BSI and BMVI: Group A, < 2; Group B, 2–3.9; Group C, 4–7.9; and Group D, ≥ 8 [8], and the association of ALP and PSA among the four

groups (Groups A–D) at four levels (SUV, ≥ 5 to ≥ 8) was evaluated using the analysis of variance (ANOVA). Tukey's post hoc test was used to assess significant between-group differences. All statistical analyses were conducted using SPSS statistics 27 (IBM Corp., Armonk, NY, USA). A p value of < 0.05 was considered statistically significant.
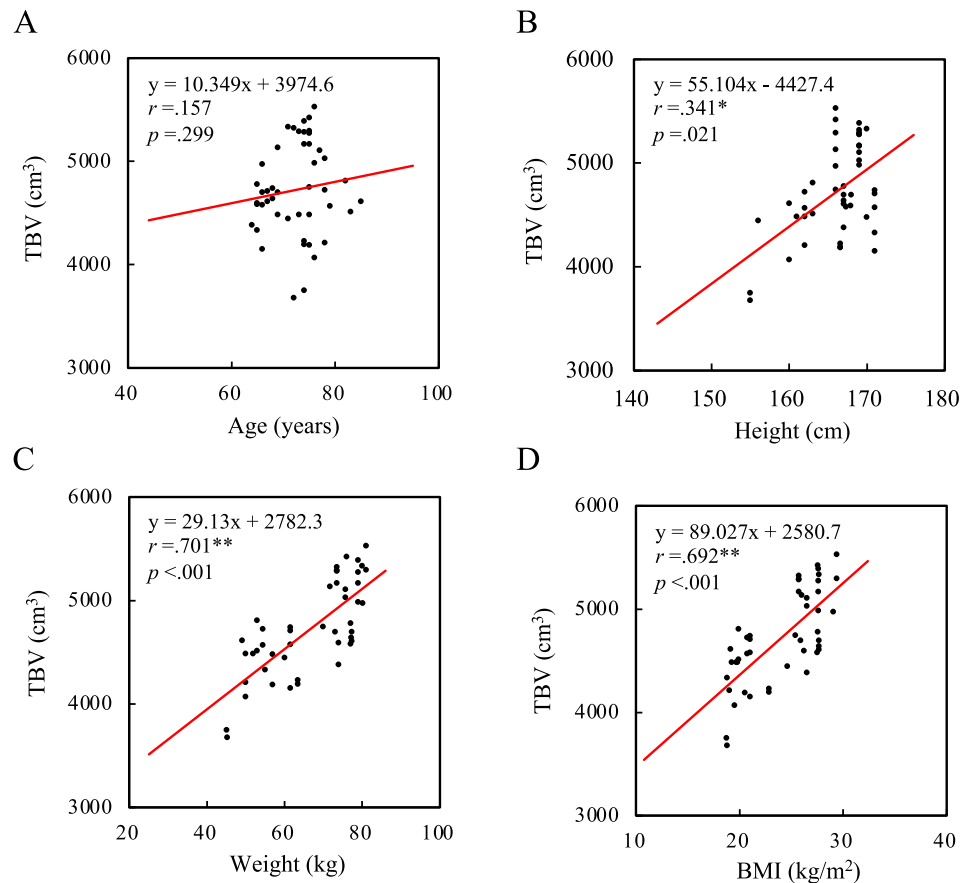
Results

The median ALP and PSA levels were 235 (range 44–524) U/L and 3.7 (range 0.010–597) ng/mL, respectively. The mean TBV was 4661.7 ± 133.8 cm^3 (median 4621.2), resulting in the mean %CV of 2.8% (range, 0.5–5.0%). Figure 2 shows scatter plots with regression lines for TBVs. TBV was correlated with height ($p = 0.021$), weight ($p < 0.001$), and BMI ($p < 0.001$) but was not correlated with age ($p = 0.299$). Especially, TBV was strongly correlated with body weight.

The median BSI and BMVI calculated with threshold values of 5–8 for SUV (BMVI$_{SUV5, 6, 7, 8}$) were 0.56, 4.23, 2.22, 1.51, and 0.55, respectively. Figure 3 shows scatter plots with regression lines and Bland–Altman analysis. When comparing BMVI and BSI, BMVI$_{SUV5–7}$ showed significantly higher values ($p < 0.001$), whereas BMVI$_{SUV8}$ showed lower values ($p = 0.666$), indicating an inverted relationship. Proportional errors were observed between BSI and BMVI$_{SUV5–8}$ ($p < 0.001$). Table 1 shows significant correlation coefficients between ALP and PSA with BSI and BMVI. The correlation between ALP and BMVI$_{SUV5}$ ($r = 0.34$, $p = 0.02$), BMVI$_{SUV6}$ ($r = 0.39$, $p = 0.008$), and BMVI$_{SUV7}$ ($r = 0.40$, $p = 0.005$) was low, while BSI ($r = 0.44$, $p = 0.002$) was moderately correlated with ALP. Moreover, a moderate correlation was observed between PSA and BSI ($r = 0.45$, $p = 0.002$) and BMVI$_{SUV8}$ ($r = 0.49$, $p < 0.001$), but a low correlation was observed between PSA and BMVI$_{SUV7}$ ($r = 0.36$, $p = 0.018$). Figure 4 shows the relationship between ALP and BSI, and BMVI$_{SUV5-8}$. Results were classified based on BSI as 38, 2, 4, and 2 scans in groups A, B, C, and D; 8, 12, 12, and 14 for BMVI$_{SUV5}$; 20, 13, 4, and 9 for BMVI$_{SUV6}$; 30, 6, 5, and 5 for BMVI$_{SUV7}$; and 40, 5, 1, and 0 for BMVI$_{SUV8}$, respectively. The statistical F values by ANOVA were 0.854 ($p = 0.472$), 1.626 ($p = 0.198$), 4.095 ($p = 0.012$), 1.919 ($p = 0.141$), and 1.053 ($p = 0.358$) for BSI, BMVI$_{SUV5}$, BMVI$_{SUV6}$, BMVI$_{SUV7}$, and BMVI$_{SUV8}$, respectively.

Figure 5 shows the results of serial BONENAVI and maximum intensity projection (MIP) images. PSA in Fig. 5b–d was significantly higher than that of the previous values, whereas ALP, BSI, and BMVI showed no obvious changes. Figure 5d, e seems to be almost identical with the extracted extent of bone metastasis, although the BMVI was higher than the BSI. Pelvic segmentation using the BONENAVI software showed overextraction below the ischial bone in all

Fig. 2 Correlation between TBV and age (**a**), height (**b**), weight (**c**), and BMI (**d**)*, $p < 0.05$; **, $p < 0.01$

A

y = 10.349x + 3974.6
$r = .157$
$p = .299$

TBV (cm^3) vs Age (years)

B

y = 55.104x − 4427.4
$r = .341*$
$p = .021$

TBV (cm^3) vs Height (cm)

C

y = 29.13x + 2782.3
$r = .701**$
$p < .001$

TBV (cm^3) vs Weight (kg)

D

y = 89.027x + 2580.7
$r = .692**$
$p < .001$

TBV (cm^3) vs BMI (kg/m^2)

whole-body images (Fig. 5a–d) because of abnormal uptake of the right ischial bone. The abnormal uptake in the fifth lumbar vertebra was consistently interpreted by the physician as a degenerative change in all four bone scintigraphy. Extraction of the cervical spine in the MIP image (Fig. 5e) was also interpreted as a degenerative change.

Another patient showed results of serial BONENAVI and MIP images in Fig. 6. PSA and BMVI were rapidly elevated from Fig. 6b–e, and ALP was elevated after Fig. 6c. However, the BSI had a high value as shown in Fig. 6e. Furthermore, bone metastases in the bilateral ribs and right femur in Fig. 6c were interpreted by the physician and diagnosed as worsening compared with previous examinations. In Fig. 6b, a gradual progressive worsening of bone metastases in the thoracic and lumbar spine, ribs, and pelvis was diagnosed. The patient received chemotherapy and was then treated with Radium-223 (Fig. 6e).

Discussion

As the bone metastasis is identified as osteoblastic in patients with prostate cancer, bone scintigraphy can visualize abnormalities as hot spots or localized uptake. Although SPECT/CT images are indispensable in obtaining a quantitative

index on the extent of abnormal bone-avid tracer uptake with high accuracy, few studies have been conducted on this subject. In the present study, we attempted to extract bone metastases through the SUV threshold value in quantitative SPECT/CT images to calculate the BMVI so that the extent of bone metastases can be predicted accurately. BMVI could be extremely reproducible in calculating the entire bone volume and was highly value than BSI when calculated with the SUV threshold of 5–7. The BMVI may be associated with ALP when calculated with the threshold value of 6 for SUV even in a small number of patients.

The first step toward more accurate assessment of the extent of bone metastases in the entire skeleton should be accurate and reproducible measurement the skeletal volume. Since BSI calculation estimates the weight of each bone region segmented by part from the whole-body planar image and is the percentage of the weight of the entire skeleton and bone metastases, the segmentation accuracy is a pivotal factor [2]. The case in Fig. 5 showed that the pelvic segmentation was incorrect because of the overextraction of the ischial bone (Fig. 5a–d) and underextraction of the iliac bone (Fig. 5a, c). With our proposed method, the volume data of CT and SPECT images could be used to complement with each other, thus enabling the measurement of the entire skeletal volume with a lower variability of < 3%. This benefit

Fig. 3 Scatter plots and Bland–Altman plots to compare BSI and BMVI with SUV threshold values of 5–8. Solid and dashed blue lines in Bland–Altman plots show mean difference and 95% confidence interval, respectively
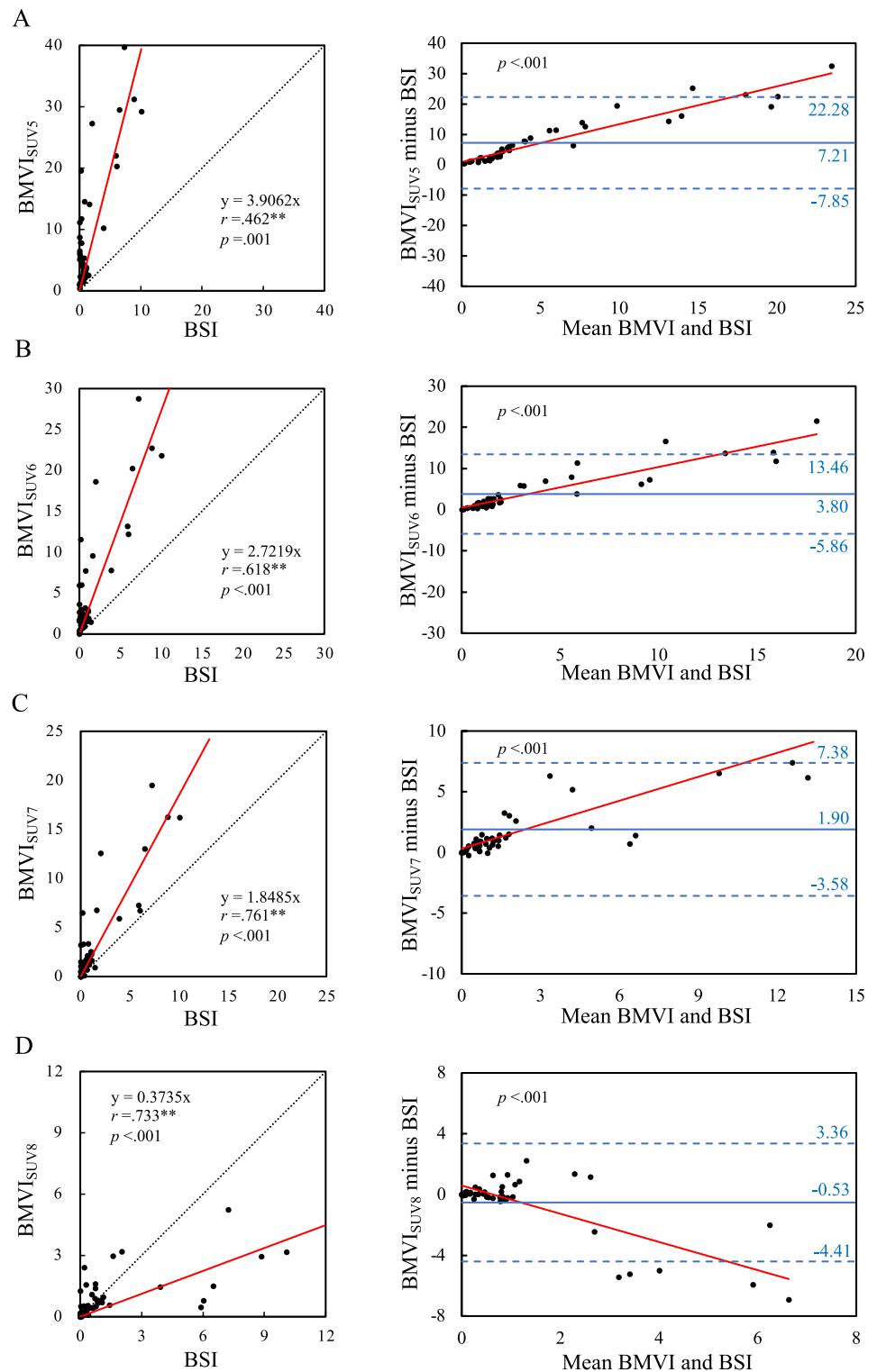
has also been used to extract bone lesions. TBV is most strongly correlated with body weight (Fig. 2), a result that seems almost appropriate when estimated from the relative weights of each bone [23].

Bone metastases in the spine and pelvis have significantly higher SUVs than degenerative changes, with the mean SUVs of bone metastases higher in the pelvis, spine, extremities, scapular girdle, and ribs, respectively [24]. Lowering the SUV threshold value increases not only the sensitivity of lesion detection but also false positives, whereas the relationship is reversed as the SUV threshold is increased [22]. The setting of the threshold value will be a tradeoff between

Table 1 Correlation coefficients among ALP, PSA, BSI, and BMVI$_{SUV5–8}$

	BSI	BMVI$_{SUV5}$	BMVI$_{SUV6}$	BMVI$_{SUV7}$	BMVI$_{SUV8}$
ALP	0.44	0.34	0.39	0.40	n.s
PSA	0.45	n.s	n.s	0.36	0.49

n.s, not significant

sensitivity and specificity, setting SUV 6 as the threshold value that correlated with ALP and had the highest statistical *F* value. In Umeda et al.'s report [22] on the optimal SUV threshold value for the assessment of bone metastasis using TBU, SUV 7 was found to be optimal, but SUV 6 showed almost the same results and was superior to 7 in sensitivity. Our results showing the correlation with ALP demonstrated a stronger correlation with the SUV threshold value of 6, but the threshold value of 7 may be better, although not significantly different, according to Group C in Fig. 4b, c. Setting the SUV threshold value to 8 underestimated the EOD (Fig. 3d), and even when set to 6 extracted, only a few bone metastases in the ribs were identified (Fig. 6); nevertheless, setting to 5 would substantially extract other bone metastases. This problem may be improved with the variable SUV threshold values for each segment of the body. Tsujimoto et al. proposed a lesion detection program using SPECT/CT images that manually segment body parts using CT images and automatically detect abnormal uptake of SPECT images by determining the threshold value for detecting lesions based on the standard deviation of SPECT count for individual patients [20]. This program is excellent in that the normal tracer uptake at each body part is considered different; however, the objectivity may be lacking in threshold values for detecting lesions, which may vary from patient to patient. This condition occurs, because the uptake is likely to be underestimated in patients with multiple bone metastases such as super bone scan because of the increased uptake throughout the spine and pelvis. Our method, which uses the SUV threshold value to detect lesions, can improve this problem and is a reasonable method that allows the use of freeware. In the future, establishing a program that can vary the SUV threshold value according to body parts is warranted.

Another advantage of using SPECT/CT images to detect abnormal uptakes would be to avoid anatomical overlap. Lesion detection on whole-body planar images may not be accurate because of bone-on-bone overlap, and bone overlap in the kidneys, ureters, and bladder containing radioactive urine, as well as radioactivity contamination [25]. Patients with prostate cancer often have difficulty voiding properly. In Fig. 5, if an abnormal uptake was observed in the sacrum, no detection would have been possible, because of the radioactive urine in the bladder. Furthermore, in Fig. 5a, urine in the

renal pelvis was detected as a less likely malignant uptake in the left rib. The region may not be accurately extracted even on curved rib contours (Fig. 6e). Moreover, planar images have lower contrast than SPECT images, which cannot be corrected for attenuation, scatter, and blurring because of collimator apertures.

The BMVI at SUV threshold values of 5–7 was clearly higher than BSI, although significantly correlated. Since the scan range of BMVI measurements was from the cervical spine to the pelvis, where a higher frequency of bone metastases may have been present, the proportion of bone diseases was relatively higher than the entire skeleton. This may be part of the reason why BMVI was higher than BSI, which measures the femur from the skull. However, although our study was based on a small number of patients, considering that it included patients with underestimated BSI, the higher BMVI may be consistent. Wakabayashi et al. reported that BSI had a moderate correlation with bone ALP and a low correlation with logarithmic PSA [8]. The proportion of patients with visceral metastases in our study appears to be lower than that in their study because the patients were treated with Radium-223, as well as the median PSA is markedly lower than that obtained in their study, but our results also showed a moderate correlation between BSI and ALP and PSA (Table 1). In their study, because over half of the patients were classified in group A, no significant difference in the relationship between groups A and B with lower BSI was found in bone ALP. This trend was also observed in our results (Fig. 4e). Nevertheless, BMVI$_{SUV6}$ significantly differed between these groups. This difference may be important in predicting patient prognosis [26]. BMVI$_{SUV6}$ had the highest ALP and statistical *F* value, and BMVI$_{SUV7}$ correlated with both ALP and PSA. Optimization of the SUV threshold value needs to be investigated in detail in the future.

The role of bone scintigraphy is very important because of its expected 10 year mortality rate of 90% if bone metastases are present at the initial diagnosis [14]. Unfortunately, the sensitivity and specificity of whole-body planar images are not that high, which may be improved by BONENAVI. Moreover, the survival risk of patients with prostate cancer classified by BSI could be clearly stratified [27, 28]. The sensitivity and specificity of BSI can be improved by classifying lesions as benign or malignant by physicians rather than by the fully automatic method; however, physicians' subjectivity may cause interobserver variation in the BSI [14]. Furthermore, the lower the EOD grade of the patient, the lower the diagnostic accuracy of both BONENAVI and the physician. Many lesions may not be detected by BONE-NAVI as shown in Fig. 6. BMVI$_{SUV6}$ may allow early risk stratification of patients with lower BSI who show equivocal uptake on whole-body images. Just as BSI can be automatically calculated, TBV and the total MBV can also be
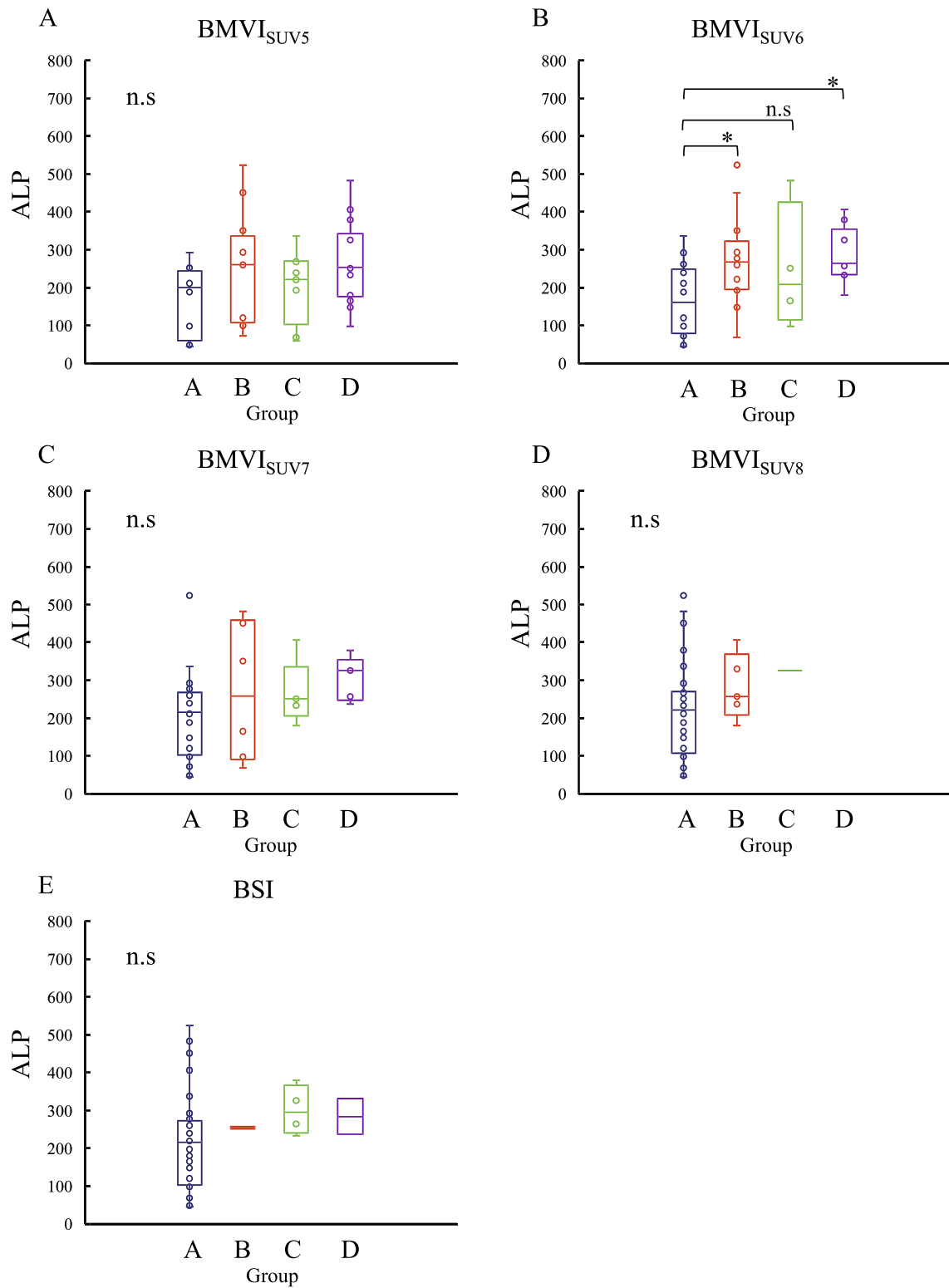
Fig. 4 Relationship among ALP and BMVI$_{SUV5}$ (**a**), BMVI$_{SUV6}$ (**b**), BMVI$_{SUV7}$ (**c**), BMVI$_{SUV8}$ (**d**), and BSI (**e**). n.s, not significant; *, $p < 0.05$

automatically calculated using a freeware; therefore, BMVI can be obtained by simply dividing them. Our proposed method would also achieve a similar high agreement as BSI, because no observer subjectivity is required.
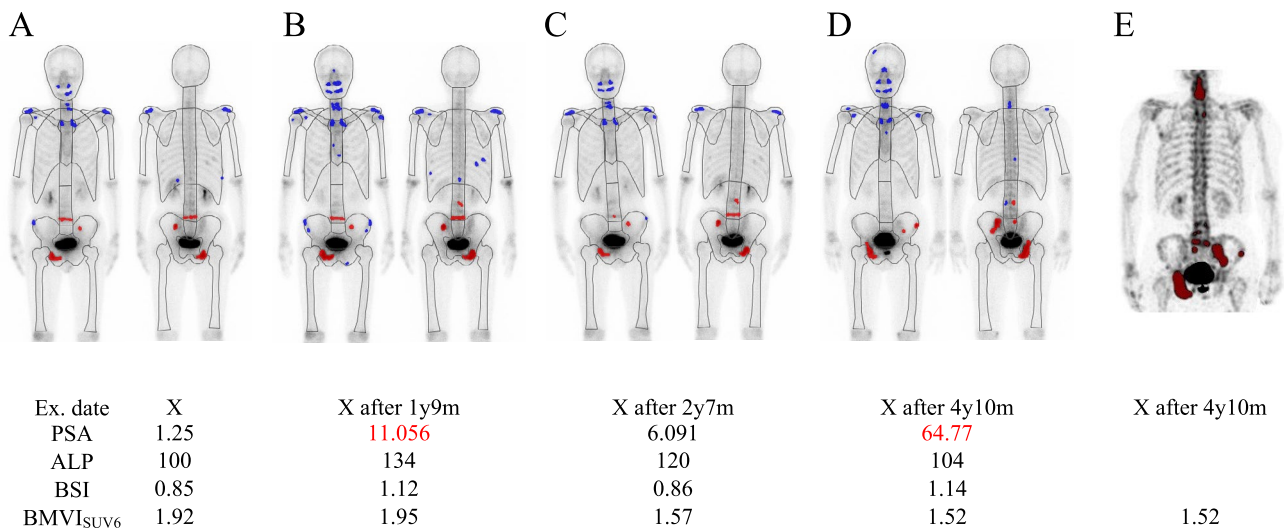
Fig. 5 Bone scintigraphy of a man in his 70 s at the initial (**a**) and follow-up (**b**–**d**) examinations MIP image (**e**) at the same examination as (**d**). Serial PSA, ALP, BSI, and $BMVI_{SUV6}$ values are shown, and values that showed an increase of > 50% from the previous value are shown in red

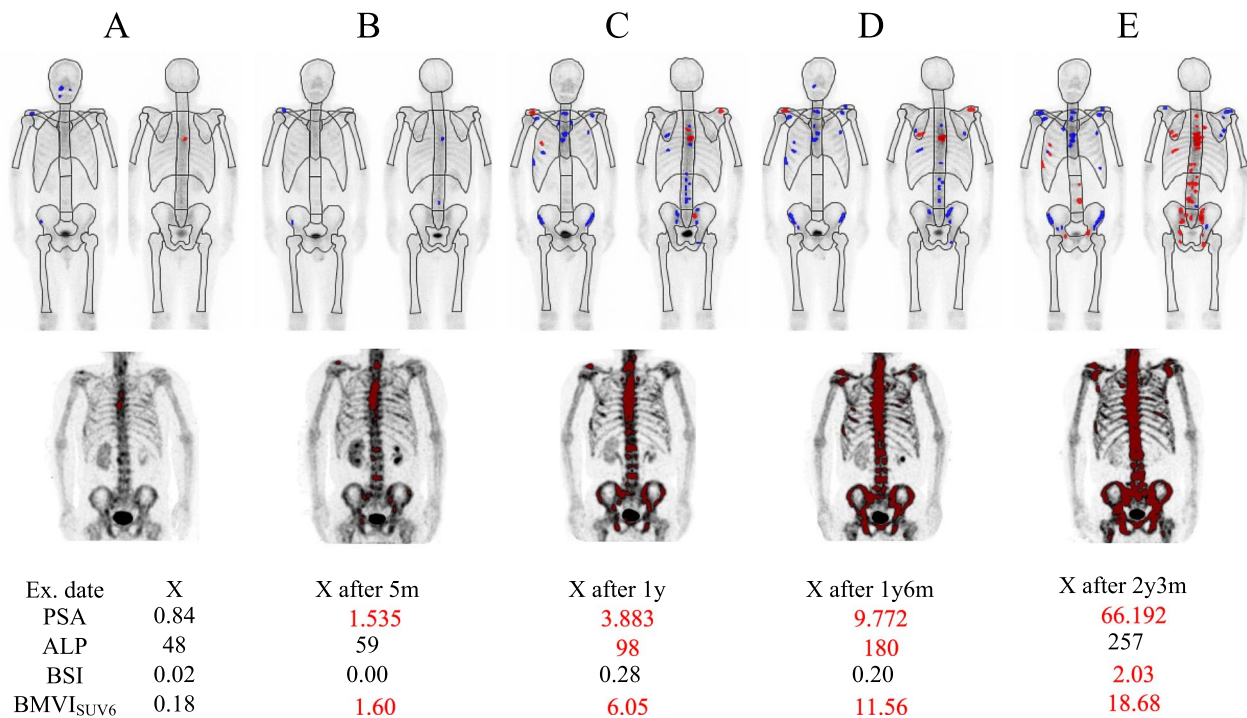| Ex. date	X	X after 1y9m	X after 2y7m	X after 4y10m	X after 4y10m
PSA	1.25	11.056	6.091	64.77	
ALP	100	134	120	104	
BSI	0.85	1.12	0.86	1.14	
$BMVI_{SUV6}$	1.92	1.95	1.57	1.52	1.52

Fig. 6 Bone scintigraphy and MIP images of a man in his 70 s during follow-up examinations. Serial PSA, ALP, BSI, and $BMVI_{SUV6}$ values are shown, and values that showed an increase of > 50% from the previous value are shown in red

Ex. date	X	X after 5m	X after 1y	X after 1y6m	X after 2y3m
PSA	0.84	1.535	3.883	9.772	66.192
ALP	48	59	98	180	257
BSI	0.02	0.00	0.28	0.20	2.03
$BMVI_{SUV6}$	0.18	1.60	6.05	11.56	18.68

The main limitations of this study are the small number of patients and the lack of false-positive assessments because only patients on Radium-223 therapy were included in the study. Whole-body planar images can be acquired in every institution, whereas SPECT/CT systems have not been fully available at present. Even if the systems were available, SPECT requires prolonged examination time and CT increases the radiation dose. Because the skull and femur were excluded from the scanning range for the BMVI calculation in the present study, extending the scanning range would make a greater contribution to predicting the prognosis. These problems will be improved by imaging technologies such as high-speed SPECT acquisition [29–31] and low-dose CT technology.

Conclusions

We proposed a new index to assess the extent of bone metastases using SPECT/CT images. BMVI calculated with an SUV threshold value of 6 was found to be correlated with ALP and showed higher value than BSI, suggesting that BMVI may be improved the low sensitivity of BSI, especially in patients with low EOD grades. Further studies are needed to evaluate the correlation between BMVI and prognosis in more patients.

Declarations

Conflict of interest The authors have no conflicts of interest to disclose.

References

1. Ozu C, Nakashima J, Horiguchi Y, Oya M, Ohigashi T, Murai M. Prediction of bone metastases by combination of tartrate-resistant acid phosphatase, alkaline phosphatase and prostate specific antigen in patients with prostate cancer. Int J Urol. 2008;15:419–22.
2. Erdi YE, Humm JL, Imbriaco M, Yeung H, Larson SM. Quantitative bone metastases analysis based on image segmentation. J Nucl Med. 1997;38:1401.
3. Imbriaco M, Larson SM, Yeung HW, Mawlawi OR, Erdi Y, Venkatraman ES, et al. A new parameter for measuring metastatic bone involvement by prostate cancer: the bone scan index. Clin Cancer Res. 1998;4:1765–72.
4. Dennis ER, Jia X, Mezheritskiy IS, Stephenson RD, Schoder H, Fox JJ, et al. Bone scan index: a quantitative treatment response biomarker for castration-resistant metastatic prostate cancer. J Clin Oncol. 2012;30:519–24.
5. Ulmert D, Kaboteh R, Fox JJ, Savage C, Evans MJ, Lilja H, et al. A novel automated platform for quantifying the extent of skeletal tumour involvement in prostate cancer patients using the bone scan index. Eur Urol. 2012;62:78–84.
6. Horikoshi H, Kikuchi A, Onoguchi M, Sjostrand K, Edenbrandt L. Computer-aided diagnosis system for bone scintigrams from Japanese patients: importance of training database. Ann Nucl Med. 2012;26:622–6.
7. Nakajima K, Nakajima Y, Horikoshi H, Ueno M, Wakabayashi H, Shiga T, et al. Enhanced diagnostic accuracy for quantitative bone scan using an artificial neural network system: a Japanese multi-center database project. EJNMMI Res. 2013;3:83.
8. Wakabayashi H, Nakajima K, Mizokami A, Namiki M, Inaki A, Taki J, et al. Bone scintigraphy as a new imaging biomarker: the relationship between bone scan index and bone metabolic markers in prostate cancer patients with bone metastases. Ann Nucl Med. 2013;27:802–7.
9. Armstrong AJ, Anand A, Edenbrandt L, Bondesson E, Bjartell A, Widmark A, et al. Phase 3 assessment of the automated bone scan index as a prognostic imaging biomarker of overall survival in men with metastatic castration-resistant prostate cancer: a secondary analysis of a randomized clinical trial. JAMA Oncol. 2018;4:944–51.
10. Kaboteh R, Damber JE, Gjertsson P, Hoglund P, Lomsky M, Ohlsson M, et al. Bone scan index: a prognostic imaging biomarker for high-risk prostate cancer patients receiving primary hormonal therapy. EJNMMI Res. 2013;3:9.
11. Sadik M, Suurkula M, Hoglund P, Jarund A, Edenbrandt L. Improved classifications of planar whole-body bone scans using a computer-assisted diagnosis system: a multicenter, multiple-reader, multiple-case study. J Nucl Med. 2009;50:368–75.
12. Meirelles GS, Schoder H, Ravizzini GC, Gonen M, Fox JJ, Humm J, et al. Prognostic value of baseline [18F] fluorodeoxy-glucose positron emission tomography and 99 mTc-MDP bone scan in progressing metastatic prostate cancer. Clin Cancer Res. 2010;16:6093–9.
13. Poulsen MH, Rasmussen J, Edenbrandt L, Høilund-Carlsen PF, Gerke O, Johansen A, et al. Bone scan index predicts outcome in patients with metastatic hormone-sensitive prostate cancer. BJU Int. 2016;117:748–53.
14. Takahashi Y, Yoshimura M, Suzuki K, Hashimoto T, Hirose H, Uchida K, et al. Assessment of bone scans in advanced prostate carcinoma using fully automated and semi-automated bone scan index methods. Ann Nucl Med. 2012;26:586–93.
15. Utsunomiya D, Shiraishi S, Imuta M, Tomiguchi S, Kawanaka K, Morishita S, et al. Added value of SPECT/CT fusion in assessing suspected bone metastasis: comparison with scintigraphy alone and nonfused scintigraphy and CT. Radiology. 2006;238:264–71.
16. Rager O, Nkoulou R, Exquis N, Garibotto V, Tabouret-Viaud C, Zaidi H, et al. Whole-body SPECT/CT versus planar bone scan with targeted SPECT/CT for metastatic workup. Biomed Res Int. 2017;2017:7039406.
17. Palmedo H, Marx C, Ebert A, Kreft B, Ko Y, Turler A, et al. Whole-body SPECT/CT for bone scintigraphy: diagnostic value and effect on patient management in oncological patients. Eur J Nucl Med Mol Imaging. 2014;41:59–67.
18. Lofgren J, Mortensen J, Rasmussen SH, Madsen C, Loft A, Hansen AE, et al. A prospective study comparing ^{99m}Tc-hydroxy-ethylene-diphosphonate planar bone scintigraphy and whole-body SPECT/CT with ^{18}F-fluoride PET/CT and ^{18}F-fluoride PET/MRI for diagnosing bone metastases. J Nucl Med. 2017;58:1778–85.
19. Kaneta T, Ogawa M, Daisaki H, Nawata S, Yoshida K, Inoue T. SUV measurement of normal vertebrae using SPECT/CT with Tc-99 m methylene diphosphonate. Am J Nucl Med Mol Imaging. 2016;6:262–8.
20. Tsujimoto M, Teramoto A, Ota S, Toyama H, Fujita H. Automated segmentation and detection of increased uptake regions in bone scintigraphy using SPECT/CT images. Ann Nucl Med. 2018;32:182–90.
21. Kuji I, Yamane T, Seto A, Yasumizu Y, Shirotake S, Oyama M. Skeletal standardized uptake values obtained by quantitative SPECT/CT as an osteoblastic biomarker for the discrimination of active bone metastasis in prostate cancer. Eur J Hybrid Imaging. 2017;1:2.
22. Umeda T, Koizumi M, Fukai S, Miyaji N, Motegi K, Nakazawa S, et al. Evaluation of bone metastatic burden by bone SPECT/CT in metastatic prostate cancer patients: defining threshold value for total bone uptake and assessment in radium-223 treated patients. Ann Nucl Med. 2018;32:105–13.
23. Report of the task group on reference man. Ann ICRP. 1979;3(1–4):iii.
24. Tabotta F, Jreige M, Schaefer N, Becce F, Prior JO, Nicod LM. Quantitative bone SPECT/CT: high specificity for identification of prostate cancer bone metastases. BMC Musculoskelet Disord. 2019;20:619.
25. Shafi A, Thorsson O, Edenbrandt L. New routine for nuclear medicine technologists to determine when to add SPECT/CT to a whole-body bone scan. J Nucl Med Technol. 2014;42:28–32.
26. Nakajima K, Edenbrandt L, Mizokami A. Bone scan index: a new biomarker of bone metastasis in patients with prostate cancer. Int J Urol. 2017;24:668–73.

27. Sabbatini P, Larson SM, Kremer A, Zhang ZF, Sun M, Yeung H, et al. Prognostic significance of extent of disease in bone in patients with androgen-independent prostate cancer. J Clin Oncol. 1999;17:948–948.

28. Miyoshi Y, Yoneyama S, Kawahara T, Hattori Y, Teranishi J, Kondo K, et al. Prognostic value of the bone scan index using a computer-aided diagnosis system for bone scans in hormone-naive prostate cancer patients with bone metastases. BMC Cancer. 2016;16:128.

29. Zacho HD, Manresa JAB, Aleksyniene R, Ejlersen JA, Fledelius J, Bertelsen H, et al. Three-minute SPECT/CT is sufficient for the assessment of bone metastasis as add-on to planar bone scintigraphy: prospective head-to-head comparison to 11-min SPECT/CT. EJNMMI Res. 2017;7:1.

30. Yamane T, Takahashi M, Matsusaka Y, Fukushima K, Seto A, Kuji I, et al. Satisfied quantitative value can be acquired by short-time bone SPECT/CT using a whole-body cadmium-zinc-telluride gamma camera. Sci Rep. 2021;11:24320.

31. Ichikawa H, Miyaji N, Onoguchi M, Shibutani T, Nagaki A, Kato T, et al. Feasibility of ultra-high-speed acquisition in xSPECT bone algorithm: a phantom study with advanced bone SPECT-specific phantom. Ann Nucl Med. 2022;36:183–90.